*ICLASS 2009, 11th Triennial International Annual Conference on Liquid Atomization and Spray Systems, Vail, Colorado USA, July 2009*

# Adaptive spectral refinement for accurate simulations of turbulent multiphase flows

Olivier Desjardins*
Department of Mechanical Engineering
University of Colorado, Boulder, CO 80309-0427

**Abstract**

This work presents an extension of the spectrally refined interface (SRI) approach introduced in [J. Comp. Phys. 228 (2009) 1658–1677] for simulating turbulent multiphase flows. Based on pseudo-spectral sub-grid refinement of a level set function using quadrature points in each computational cell, the SRI methodology was shown to combine excellent accuracy with good numerical robustness. The increased resolution obtained from the introduction of quadrature points makes SRI a method of choice for tracking small-scale liquid structures. Several improvements to this method are presented in this paper. First, a standard signed distance level set function is used instead of a hyperbolic tangent function, which is found to improve significantly the accuracy of curvature computation. Then, the communication pattern between refined cells is simplified, leading to a straightforward implementation. Finally, the number of quadrature points is allowed to vary from cell to cell, enabling the sub-cell resolution to be adapted to the interface topology. Two strategies for adaptive refinement are combined, namely refinement based on the distance from the phase-interface, and refinement based on the local front curvature. The new adaptive SRI scheme (ASRI) is easier to implement, and is shown to be more accurate and computationally efficient than the original SRI approach.

## Introduction

Simulating turbulent multiphase flows, which are found in engineering applications such as fuel injection for combustion systems, remains a daunting task. Robust handling of large density ratios, precise modeling of surface tension forces, and accurate tracking of the phase-interface are but a few of the design objectives of a successful numerical scheme for turbulent two-phase flows. Classically, the first method of choice for two-phase simulations was the volume of fluid (VOF) method [1]. However, this method has the disadvantage of requiring a geometric transport scheme, which is typically of limited accuracy. The level set (LS) method [2, 3], which allows for high order accuracy, was proposed to alleviate this issue, but usually suffers from poor conservation properties. Coupled schemes, which combine VOF and LS methods [4, 5], have been proposed to obtain both good accuracy and excellent mass conservation. However, it was realized that such schemes might not accurately predict the interfacial curvature [6]. This illustrates the conflicting nature of these design objectives.

Recently, Desjardins and Pitsch [7] proposed a novel approach based on spectral refinement of a level set function (SRI). The SRI method uses a level set function to localize the phase-interface, and provides sub-cell resolution in the form of quadrature points located inside each flow solver cell. In order to alleviate the CFL restrictions associated with mesh refinement, a semi-Lagrangian scheme is employed to transport the level set function. In addition to providing increased local resolution, the sub-cell quadrature points allow to define a high order polynomial reconstruction of the level set function, effectively increasing the order of accuracy at the same time as the resolution. This pseudo-spectral approach to sub-grid refinement of a level set function was found to provide both excellent accuracy and excellent numerical robustness.

This work aims at extending the SRI approach. Several modifications are proposed, leading to an overall improvement over the original scheme. First, the level set function, which was taken to be a hyperbolic tangent function in the original SRI method, is replaced here by a standard signed distance level set function. This modification, combined with new curvature computation schemes, was found to lead to a large reduction in curvature errors. Then, the interaction between refined cells is significantly simplified. In the original SRI method, ghost quadrature points were used, which required the implementation of a fairly complex multi-level communication scheme. This aspect is entirely removed in the new scheme, leading to a much

* *E-mail address:* desjardi@colorado.edu

simpler implementation. Finally, and most importantly, the SRI scheme is modified to allow for a variable number of quadrature points per cell. This added flexibility enables the user to tailor the sub-cell refinement to the interface shape, effectively providing dynamically adaptive refinement of the level set function. Two refinement strategies are combined in this work, namely refinement based on the distance from the phase-interface, and refinement based on the local front curvature. It is shown that the resulting adaptive SRI (ASRI) scheme is more accurate, more computationally efficient, and simpler to implement than the original SRI method, making it a method of choice for high resolution interfacial transport. Because of the limited length of this paper, only an brief overview of some of the proposed improvements and numerical tests are presented here.

## Mathematical description

Many gas-liquid flows can be described using the continuity and Navier-Stokes equations. Assuming both phases are incompressible, *i.e.* $\nabla \cdot \boldsymbol{u} = 0$, the continuity equation is written

$$\frac{D\rho}{Dt} = \frac{\partial \rho}{\partial t} + \boldsymbol{u} \cdot \nabla \rho = 0, \tag{1}$$

where $\boldsymbol{u}$ is the velocity field and $\rho$ is the density. The Navier-Stokes equations are written

$$\frac{\partial \boldsymbol{u}}{\partial t} + \boldsymbol{u} \cdot \nabla \boldsymbol{u} = -\frac{1}{\rho}\nabla p + \frac{1}{\rho}\nabla \cdot \left(\mu \left[\nabla \boldsymbol{u} + \nabla \boldsymbol{u}^t\right]\right) + \boldsymbol{g}, \tag{2}$$

where $p$ is the pressure, $\boldsymbol{g}$ is the gravitational acceleration, and $\mu$ is the dynamic viscosity.

The material properties are considered to be constant in each phase. The subscript $l$ is used to describe the density and the viscosity in the liquid, respectively $\rho_l$ and $\mu_l$. Similarly, the subscript $g$ corresponds to the density and the viscosity in the gas, respectively $\rho_g$ and $\mu_g$. It is convenient to introduce the jump of these quantities across the phase-interface $\Gamma$, defined by $[\rho]_\Gamma = \rho_l - \rho_g$ and $[\mu]_\Gamma = \mu_l - \mu_g$. In the absence of mass transfer between the two phases, the velocity field is continuous across $\Gamma$, *i.e.* $[\boldsymbol{u}]_\Gamma = 0$. In contrast, the existence of surface tension forces will lead to a discontinuity in the normal stresses at the gas-liquid interface. This translates into a pressure jump that can be expressed as

$$[p]_\Gamma = \sigma\kappa + 2\,[\mu]_\Gamma\, \boldsymbol{n}^t \cdot \nabla \boldsymbol{u} \cdot \boldsymbol{n}, \tag{3}$$

where $\sigma$ is the surface tension coefficient, $\kappa$ is the curvature of the phase-interface, and $\boldsymbol{n}$ is the phase-interface normal.

## Adaptive spectrally refined interface (ASRI) approach

The original SRI approach was presented in detail in Desjardins and Pitsch [7]. We recall here the main concepts behind this method, and introduce several modifications to the original scheme.

*Level set methodology.* Solving Eq. 1 for the discontinuous density field $\rho$ is numerically challenging. However, noting that Eq. 1 simply states that the density undergoes material transport at the flow velocity $\boldsymbol{u}$, one can solve instead an equation for the material transport of the phase-interface $\Gamma$. The level set method [2, 3] achieves this by introducing an auxiliary function $G(\boldsymbol{x}, t)$, called level set function, such that $\Gamma$ is implicitly defined as the iso-surface $G(\boldsymbol{x}, t) = G_0$. Then, Eq. 1 can be replaced by

$$\frac{DG}{Dt} = \frac{\partial G}{\partial t} + \boldsymbol{u} \cdot \nabla G = 0. \tag{4}$$

Provided that the level set function $G$ is smooth, numerical integration of Eq. 4 is straightforward. However, in the absence of any diffusion process, ensuring that $G$ remains a smooth function requires an additional step, called re-initialization. This re-initialization step aims at re-setting $G$ to a prescribed smooth function while minimizing the displacement of the $G_0$ iso-surface. The level set function $G$ is often chosen as the signed distance to the phase-interface described by the iso-surface $G(\boldsymbol{x}, t) = G_0 = 0$, *i.e.*

$$|G(\boldsymbol{x}, t)| = |\boldsymbol{x} - \boldsymbol{x}_\Gamma|, \tag{5}$$

where $\boldsymbol{x}_\Gamma$ corresponds to the point on the interface that is closest to $\boldsymbol{x}$, and $G(\boldsymbol{x},t) > 0$ on one side of the interface, and $G(\boldsymbol{x},t) < 0$ on the other side. Two main approaches have been proposed to force $G$ to be this signed distance function. For re-initialization, a partial differential equation which admits a signed distance function as steady-state solution can be solved [8], or a geometrical scheme such as the fast marching method (FMM) can be used [2, 9].

*Pseudo-spectral sub-cell reconstruction.* In order to enable sub-cell resolution inside a flow solver cell, a polynomial reconstruction of the level set function $G$ is here generated by introducing $p_d$ Gauss-Lobatto quadrature points [10, 11] per direction $d$, where $d \in \{x, y, z\}$. These points correspond to the locations where the nodal values of the level set function $G$ are specified. The Gauss-Lobatto quadrature points used here are based on the Legendre family of orthogonal polynomials.

Because of the structured environment which is considered here, one index will be used per direction to describe the computational space. Let the $G$ value of the quadrature point $(l, m, n)$ of the flow solver cell $(i, j, k)$ be denoted $G^{l,m,n}_{i,j,k}$, and its position vector $\boldsymbol{x}^{l,m,n}_{i,j,k}$. Consider a cell of unit size in direction $d$, and let $r_l$ with $l \in [\![1, p_d]\!]$ represent the position of the $l^{\text{th}}$ quadrature point in that direction, for which then $r_1 = 0$ and $r_{p_d} = 1$. Similarly, let the flow solver mesh be defined by the location of the lower left, proximal corner $(x_i, y_j, z_k)$ for each cell $(i, j, k)$. Using these definitions, the cardinal functions for algebraic interpolation in direction $d$, $L^\alpha_{p_d}(\boldsymbol{x})$, can be defined for $\alpha \in [\![1, p_d]\!]$ by

$$L^\alpha_{p_d}(r) = \frac{\prod_{\beta=1,\beta\neq\alpha}^{p_d}(r - r_\beta)}{\prod_{\beta=1,\beta\neq\alpha}^{p_d}(r_\alpha - r_\beta)}. \tag{6}$$

Then, the level set function reconstruction within cell $(i, j, k)$ can be written

$$G_{i,j,k}(x, y, z) = \sum_{l=1}^{p_x} L^l_{p_x}\left(\frac{x - x_i}{x_{i+1} - x_i}\right) \sum_{m=1}^{p_y} L^m_{p_y}\left(\frac{y - y_j}{y_{j+1} - y_j}\right) \sum_{n=1}^{p_z} L^n_{p_z}\left(\frac{z - z_k}{z_{k+1} - z_k}\right) G^{l,m,n}_{i,j,k}. \tag{7}$$

Note that this reconstruction is of order $p_d - 1$ in direction $d$.

By construction, the Gauss-Lobatto quadrature generates points at the cell faces, leading to overlapping quadrature nodes between cells. In Desjardins and Pitsch [7], the overlapping nature of the quadrature was handled by introducing ghost quadrature nodes. While this treatment allowed to avoid unnecessary computations, it was also fairly complex to implement, especially in parallel. Here, no special treatment is used, and face nodes are handled like any other quadrature node, leading to a significant simplification of the implementation, at the cost of a slight redundancy in the computations. As in Desjardins and Pitsch [7], the sub-cell polynomial reconstruction is introduced only in a narrow band around the front, *i.e.* around the $G_0$ value of the level set function, as illustrated by Fig. 1.

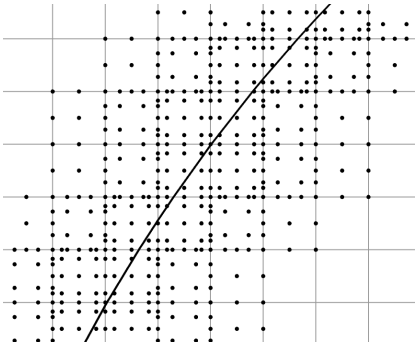

**Figure 1.** Narrow band spectral refinement around the $G_0$ iso-contour of the level set function $G$ (thick line).

*Semi-Lagrangian transport.* Classically, pseudo-spectral methods have been used to solve conservation laws by computing fluxes from the polynomials directly. While this approach is spectrally accurate, it leads to very strong restrictions in time step sizes. Here, a different approach is necessary in order to circumvent entirely the stringent CFL restrictions that arise from having a large number of sub-cell quadrature points. As in Desjardins and Pitsch [7], a semi-Lagrangian transport scheme is employed.

Instead of discretizing Eq. 4, semi-Lagrangian transport consists of observing that $G$ should be constant along the trajectory of material points evolving at velocity $\boldsymbol{u}$. Therefore, the trajectory that passes through $\boldsymbol{x}^{n+1}$ at time $t^{n+1}$ can be followed backward in time to $t^n = t^{n+1} - \Delta t$ to obtain the old location $\boldsymbol{x}^n$. The value of the level set function $G^{n+1}$ at $\boldsymbol{x}^{n+1}$ can simply be obtained by noting that $G^{n+1}\left(\boldsymbol{x}^{n+1}\right) = G^n\left(\boldsymbol{x}^n\right)$. However, in the framework of ASRI, a polynomial reconstruction is readily available in each cell. Hence, this polynomial can simply be evaluated at the old location $\boldsymbol{x}^n$, and high accuracy can be expected from the semi-Lagrangian transport.

*Stabilization technique.* Ensuring the numerical robustness of the ASRI scheme is fundamental. To this purpose, the choice is made to revert back to local tri-linear interpolations between quadrature nodes when the polynomial is found to oscillate. Very simple and straightforward to implement, the idea behind this approach is to check that each polynomial evaluation lies between the level set values of the 8 closest quadrature points. If it is indeed the case, then the polynomial evaluation is considered valid, and therefore trusted. If it is not the case, then it means that locally the polynomial reconstruction is oscillating, and therefore tri-linear interpolation is used instead. This was found to be sufficient to remove all oscillations from the computed solutions. Moreover, it was also found that it is only rarely necessary to revert to tri-linear interpolation, and therefore it is expected to have little impact on the accuracy of the method, especially since the second order error introduced in this tri-linear interpolation step is at the sub-cell level.

*Transfer to the flow solver mesh.* While the level set function is transported at the sub-grid level, it is also necessary to know the values of the level set function on the flow solver mesh. This is achieved by first performing a volumetric integration of the sub-cell $G$ polynomial over each flow solver cell. This operation has the double advantage of being spectrally accurate and computationally efficient, since one only needs to know the level set values at each quadrature node as well as the integration weight associated with each nodes, which can easily be pre-computed and stored. Finally, a FMM step is used to ensure that a signed distance function is obtained on the flow solver mesh, even in cells that are not within the narrow band of refined cells.

*Curvature computation.* While the curvature can readily be computed from the reconstructed distance function on the flow solver mesh, it can also be obtained from sub-cell information. In particular, a novel curvature scheme based on algebraic moving least-square (AMLS) reconstruction has been implemented [12]. While the original algorithm uses interface information in order to fit spheres to the interface, a modified version is introduced here, that relies on a more general second order polynomial of the form $f(x,y,z) = \alpha_1 + \alpha_2 x + \alpha_3 y + \alpha_4 z + \alpha_5 x^2 + \alpha_6 y^2 + \alpha_7 z^2$. This new scheme is found to lead to an order of magnitude reduction in curvature errors compared to standard least squares fitting [7, 13, 14].

*Adaptive formulation.* As shown in Fig. 1, the level of sub-cell refinement does not have to be identical in all flow solver cells. Regions where the phase-interface is strongly convoluted would benefit from additional resolution, while regions where the interface remains essentially flat would be properly resolved with less quadrature points. Based on this observation, the local number of quadrature points $p_d$ in a given direction $d$ is allowed to vary based on

$$p_d = \max\left(\lceil p_{\max} |\kappa| \, h_d \rceil, p_{\text{def}}\right), \tag{8}$$

where $h_d$ is the local mesh size in direction $d$, $p_{\max}$ is the maximum number of quadrature points, and $p_{\text{def}}$ is the default number of quadrature points. Using this definition, the refinement varies between $p_{\max}$ in regions where the curvature is large, to $p_{\text{def}}$ elsewhere. In addition, the refinement is made a function of the distance to the interface, since maximum accuracy is necessary at the front, while the level set function $G$ is meaningless away from the interface. Consequently, the value $p_d$ given by Eq. 8 is used only for a two-cell wide layer around the interface, and one quadrature point is removed each time we move one cell further away from the interface.

## Numerical results

Several numerical tests are presented so that the accuracy and robustness of the proposed ASRI scheme can be evaluated. As in Desjardins and Pitsch [7], the Navier-Stokes solver used here is NGA [15], modified to handle two-phase flows using the ghost fluid method (GFM) [16].

*Solid body rotation of a notched disk.* In a $[-0.5, 0.5] \times [-0.5, 0.5]$ domain, a circle of radius 0.15 with a notch of height 0.25 and width 0.05, initially centered at $(0, 0.25)$, undergoes a solid body rotation at angular velocity $2\pi$. A $50^2$ flow solver grid is used, and the time step size is set to $1/200$, meaning that 200 time

steps are necessary to perform one full rotation of the circle. This leads to a CFL number close to 0.77. Figure 2 compares the exact solution with the computed solution after one rotation and after 50 rotations. ASRI naturally puts more quadrature points in the notch area, while using less quadrature points to resolve

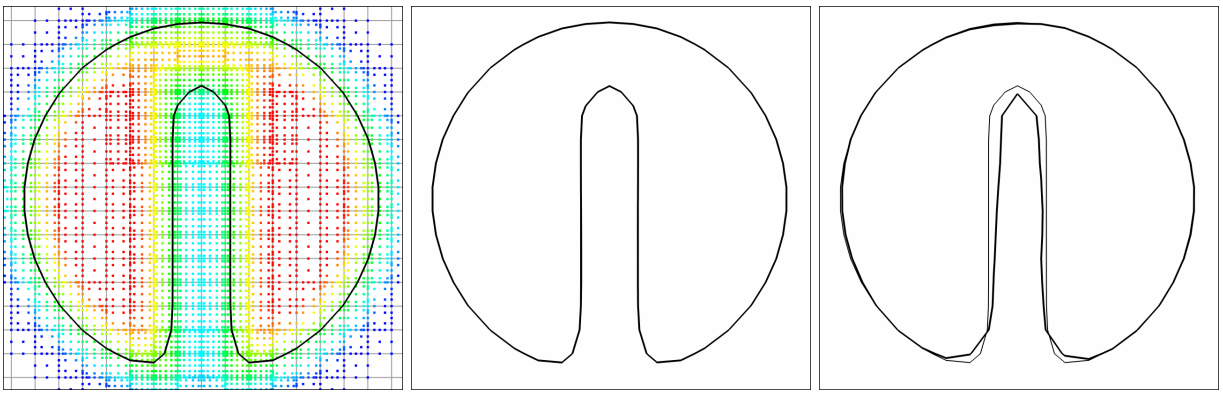

(a) (b) (c)

**Figure 2.** Solid body rotation of Zalesak's disk with $p_{\text{def}} = 5$ and $p_{\max} = 7$. (a) Exact interface location (thick line), quadrature nodes colored by the level set function, and flow solver mesh. (b) Solution after one rotation: exact solution (thin line) and ASRI solution (thick line). (c) Solution after 50 rotations: exact solution (thin line) and ASRI solution (thick line).

the circle and the region away from the interface. Even though the mesh used for this simulation is very coarse and resolves the notch on only two cells, the ASRI solution appears excellent after one rotation, and remains very satisfactory even after 50 rotations. This first result suggests that the ASRI concept enables a highly accurate description of small interfacial features, even for long time transport.

*Spurious currents.* A two dimensional drop of diameter $D = 0.4$ is placed in the center of unit size box. Initially, the velocity field is zero, but because of inaccuracies in the computation of interfacial curvature, a spurious flow will be generated. The two fluids have the same density $\rho$ and the same viscosity $\mu = 0.1$, the surface tension coefficient $\sigma$ is unity. In order to consider various importance of surface tension versus viscous forces, the Laplace number $\text{La} = 1/\text{Oh}^2 = \sigma\rho D/\mu^2$ is varied by changing the densities of both fluids, where Oh is the Ohnesorge number. To assess the intensity of the spurious currents, the Capillary number $\text{Ca} = |u_{\max}|\mu/\sigma$ is computed at a non-dimensional time $t\sigma/(\mu D) = 250$. The simulations are performed on a $32 \times 32$ mesh with $p_{\text{def}} = 5$ and $p_{\max} = 7$, and the time step size is varied to verify the capillary CFL restriction. Detailed parameters and results are reported in Table 1. The resulting capillary numbers show

| $\rho$ | 0.3 | 3 | 30 | 300 | 3000 | 30000 |
|---|---|---|---|---|---|---|
| La | 12 | 120 | 1200 | 12000 | 120000 | 1200000 |
| $\Delta t$ | 0.0006 | 0.002 | 0.006 | 0.02 | 0.06 | 0.2 |
| Ca | $2.0 \times 10^{-7}$ | $2.0 \times 10^{-7}$ | $2.1 \times 10^{-7}$ | $3.7 \times 10^{-6}$ | $7.1 \times 10^{-6}$ | $9.0 \times 10^{-6}$ |

**Table 1.** Dependence of the magnitude of parasitic currents with the Laplace number for a static droplet with surface tension on a $32 \times 32$ mesh.

little dependence on the Laplace number, and the values of Ca are found to be significantly smaller with ASRI than with SRI [7].

*Rising bubbles.* Finally, a more complex three-dimensional two-phase flow problem with topology changes is presented. In a $[-2, 2] \times [0, 8] \times [-2, 2]$ computational domain filled with liquid up to $y = 5$, two spherical gas bubbles of unit diameter are initially located at $(0, 2.15, 0)$ and $(0.5, 1, 0)$. Due to the effect of gravity, which is set to unity, these bubbles start rising, then interact, merge, and finally break the liquid-gas interface at $y = 5$. We set $\sigma = 0.0625$, $\rho_l = 1$, $\mu_l = 0.015$, and $\rho_l/\rho_g = \mu_l/\mu_g = 100$, leading to parameters similar to the simulation of Marchandise *et al.* [14]. Figure 3 shows the phase-interface shape at various times in the simulation, which is performed on a $64 \times 128 \times 32$ mesh with $p_{\text{def}} = 5$ and $p_{\max} = 7$. The trailing bubble is accelerated in the wake of the leading bubble, causing large deformation. The two bubbles then merge, and the resulting bubble generates a large protrusion at the surface of the liquid, until the thin liquid

sheet becomes under-resolved and ruptures. The bubble shape appears to be in good agreement with the simulation of Marchandise *et al.* [14]. The high resolution provided by ASRI allows to limit mass conservation errors well below 0.25% throughout the simulation.

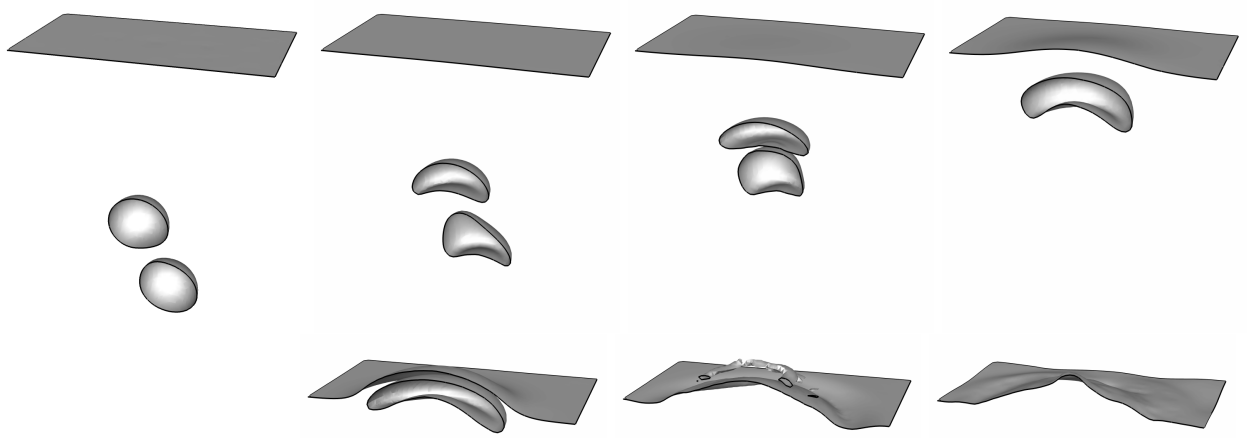

**Figure 3.** Bubbles rising and merging with ASRI. Interface location shown at one time unit intervals.

## Conclusions

Multiple improvements to the spectrally refined interface (SRI) scheme originally introduced in Desjardins and Pitsch [7] are briefly presented in this paper. The new adaptive SRI (ASRI) scheme relies on a signed distance level set function, has a simpler communication pattern, benefits from a more accurate curvature computation scheme, and enables adaptive sub-cell refinement. The accuracy and robustness of the proposed scheme is illustrated by several test cases in two and three dimensions, including topology changes. Thanks to its added accuracy and sub-cell resolution, ASRI is a scheme of choice for high resolution interfacial transport in complex two-phase flow problems such as turbulent atomization.

## References


1. Scardovelli, R. and Zaleski, S., *Ann. Rev. Fluid Mech.* 31:567–603 (1999).
2. Sethian, J. A. *Level set methods and fast marching methods*, Cambridge University Press, 1999.
3. Osher, S. and Fedkiw, R., *Level set methods and dynamic implicit interfaces*, Springer, 2003.
4. Sussman, M. and Puckett, E. G., *J. Comput. Phys.* 162:301–337 (2000).
5. van derPijl, S. P., Segal, A., and Vuik, C., *Int. J. Numer. Meth. Fluids* 47:339–361 (2005).
6. Coyajee, E., Herrmann, M., and Boersma, J. B., *Proceedings of the 2004 Summer Program, Center for Turbulence Research, Stanford, CA*, 2004.
7. Desjardins, O. and Pitsch, H., *J. Comp. Phys.* 228(5):1658–1677 (2009).
8. Peng, D., Merriman, B., Osher, S., Zhao, H., and Kang, M., *J. Comput. Phys.* 155:410–438 (1999).
9. Herrmann, M. *in Annual Research Briefs (Center for Turbulence Research, Stanford, CA)*, 2005.
10. Huang, P. G., Wang, Z. J., and Liu, Y., *AIAA Computational Fluid Dynamics Conference*, 2005.
11. Canuto, C., Hussaini, M. Y., Quarteroni, A., and Zang, T. A., *Spectral methods in fluid dynamics*, Springer-Verlag, 1988.
12. Gois, J. P., Nakano, A., Nonato, L. G., and Buscaglia, G. C., *J. Comp. Phys.* 227:9643–9669 (2008).
13. Desjardins, O., Moureau, V., and Pitsch, H., *J. Comp. Phys.* 227(18):8395–8416 (2008).
14. Marchandise, E., Geuzaine, P., Chevaugeon, N., and Remacle, J. F., *J. Comput. Phys.* 225(1):949–974 (2007).
15. Desjardins, O., Blanquart, G., Balarac, G., and Pitsch, H., *J. Comput. Phys.* 227(15):7125–7159 (2008).
16. Fedkiw, R., Aslam, T., Merriman, B., and Osher, S., *J. Comput. Phys.* 152:457–492 (1999).